A Mutual-Coupling-Suppressed Dual-Band Dual-Polarized Base Station Antenna Using Multiple Folded-Dipole Antenna

Xuekang Liu, Steven Gao, *Fellow, IEEE*, Benito Sanz-Izquierdo, Haiwei Zhang, Lehu Wen, Wei Hu, Qi Luo, *Senior Member, IEEE*, Josaphat Tetuko Sri Sumantyo, *Senior Member, IEEE*, Xue-Xia Yang, *Senior Member, IEEE*

Abstract—An interleaved shared-aperture dual-band dual-polarized base station array antenna is proposed in this paper. The lower-band (LB) element is realized by using a multiple folded-dipole antenna (MFDA) and four parasitic loops. To interpret the working principle of the MFDA, a double folded-dipole antenna (DFDA) is firstly analyzed by using the transmission line model. Then, by combining two bended DFDAs and introducing four parasitic loops, a low cross-band scattering LB element with a high out-of-band rejection level of 16 dB is obtained to cover 2.3-2.7 GHz. The higher-band (HB) element with a wide impedance bandwidth of 42.5% (3.0-4.6 GHz), a high roll-off rate (*RoR*) of 249.2 dB/GHz, and a high out-of-band rejection level of 17 dB is obtained by introducing a meander line loop, a rectangular loop and V-shaped strips near the dipole arms. By combining the proposed low scattering low-pass LB element and the high *RoR* high-pass HB element, a novel interleaved shared-aperture dual-band dual-polarized array antenna with a small frequency ratio of 1.46 and a high cross-band isolation level of 25 dB is realized. Due to the low-scattering characteristic and filtering response of the LB element, the radiation patterns of the wideband HB sub-arrays are almost unaffected.

Index Terms—Dual-band antenna, base station array antenna, dual-polarized antenna, filtering antenna.

I. INTRODUCTION

SHARED-APERTURE dual/multi-band dual-polarized array antennas have become a trend in the base station application to meet the growing need for fully integrated base stations. Although the shared-aperture design can realize a dual/multi-band array antenna with compact size and low cost, it also brings new design challenges, such as the high mutual-couplings between the closely placed antenna elements, and the cross-band scattering between the lower band (LB) and higher band (HB) elements.

To enhance the port isolations, many new methods are investigated [1]-[17]. By introducing decoupling branches [1],[2] and decouple surface [2], the mutual coupling in [1] and [2] are effectively reduced. In [3]-[5], baffles are used to improve the isolations between the elements. To obtain high isolations and good radiation performance, the structure, position, and height, of the baffle are optimized. Using filtering antennas [6]-[10] is also a popular method to obtain high isolations in the design of dual-multi-band array antenna. By properly designing the structure of the radiator [11] or integrating a filter into the transmission line [12], antenna elements with a high out-of-band rejection level can be obtained. The LB element has nearly no radiation in the operating band of the HB element, and vice versa. Thus, the port isolations in the array antenna maintain a very low level. Although the methods mentioned above can enhance the port isolations in the dual/multi-band array, the cross-band scattering is not fully addressed.

To reduce the cross-band scattering, a novel method is presented in [18]-[22]. By inserting a frequency selective surface (FSS) layer between the LB and HB elements, the cross-band scatterings in [18]-[21] are effectively reduced. In these designs, the HB elements are usually placed above the LB element. For the HB elements, the FSS layer can be equivalent to a ground plane. However, for the LB element, the FSS layer can be seen as EM transparent structure. Thus, not only high port isolation but also low cross-band scattering can be realized by using this method. However, the frequency ratios in these designs are larger than 4.

Apart from inserting the FSS layer, lifting the HB elements [23], using electromagnetic (EM) transparent LB elements [24]-[32], and introducing partially reflecting surfaces [33] can also reduce the cross-band scattering. By lifting the cavity-backed HB elements to the same plane of the LB radiator [23], the blockage effect of the LB element on the

Xuekang Liu, Benito Sanz-Izquierdo, and Lehu Wen are with the School of Engineering, University of Kent, Canterbury CT2 7NT, U.K. (e-mail: xl255@kent.ac.uk).

Steven Gao is with the Dept of Electronic Engineering, Chinese University of Hong Kong.

Haiwei Zhang is with the Huawei Technologies Ltd, China.

Wei. Hu is with National Laboratory of Science and Technology on Antennas and Microwaves, Xidian University, Xi'an, Shaanxi 710071, China.

Qi. Luo is with the School of Physics, Engineering and Computer Science, University of Hertfordshire, Hatfield AL10 9AB, U.K.

Josaphat Tetuko Sri Sumantyo is with the Center for Environmental Remote Sensing, Chiba University, Chiba 263-8522, Japan.

Xue-Xia Yang is with the School of Communication and Information Engineering, Shanghai University, Shanghai 200444, China.
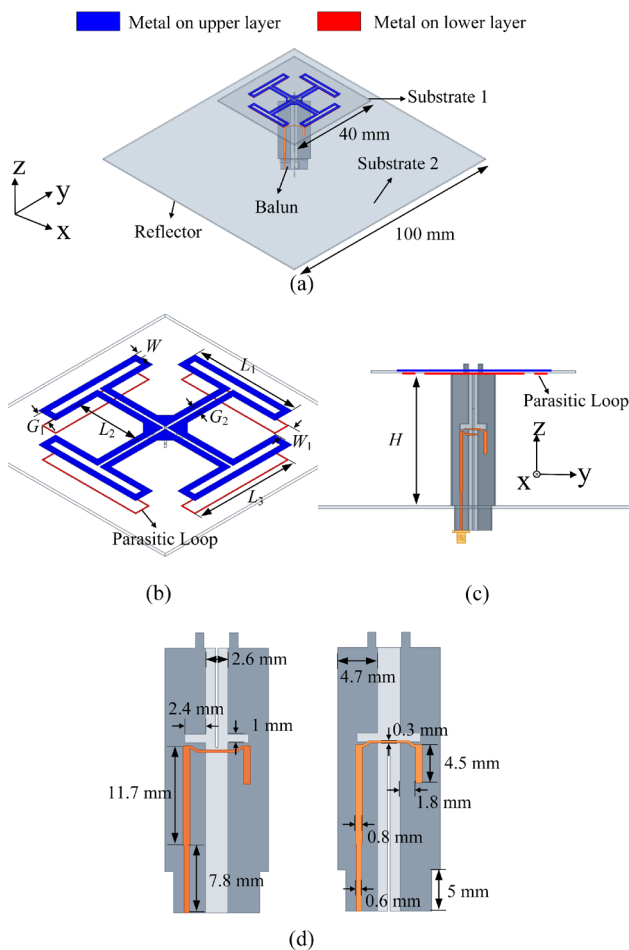
Fig. 1. Configuration of the proposed LB antenna. (a) 3D view, (b) radiator, (c) side view, and (d) Balun. Dimensions are $L_1 = 18.7$, $L_2 = 11.5$, $L_3 = 18.1$, $W = 1.1$, $W_1 = 2.7$, $G_1 = 2.2$, $G_2 = 1.5$, $H = 26$. (unit: millimeter).

radiation patterns of HB elements can be eliminated. The limitation of this method is that it is not suitable for the dual-band array antenna design with a small frequency ratio. In [24] and [25], two shared-aperture dual-band array antennas are realized by introducing branches on the radiator of LB element. By changing the length of the branches, the wave-transparent band can be easily adjusted. However, the frequency ratios of these two dual-band array antennas are larger than 2.7. By dividing the dipole arms into short sections and introducing chokes below the gaps between the short sections, a low scattering LB element is presented in [26]. Based on this LB element, a low cross-band scattering dual-band array with a small frequency ratio of 2.19 is achieved. Two low scattering LB elements are presented in [27] and [28] by introducing parasitic structures near the radiators. The combination of the radiator and the parasitic structure functions as bandpass filtering circuit. Thus, at their resonant frequencies, the HB EM wave can be transmitted through the LB element without being affected. In [30] and [31], by using the FSS element as a radiator, two low scattering LB elements are proposed. Based on these wave-transparent LB elements, two low cross-band scattering array antennas with reduced frequency ratios (1.58 and 1.42) are realized. However, the
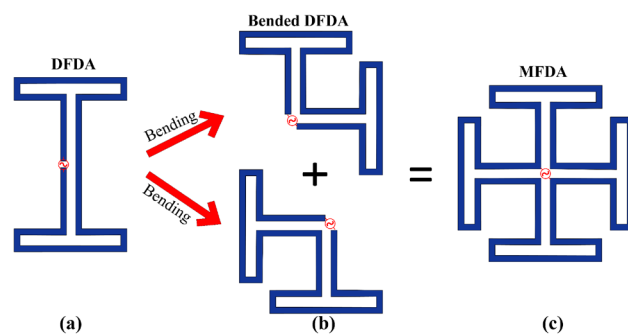

Fig. 2. Evolution of the MFDA.

wave-transparent band of these structures are relatively narrow.

In this paper, an interleaved shared-aperture dual-band dual-polarized array antenna with low frequency ratio (1.46), low cross-band scattering, wide wave-transparent band and high isolations is proposed for base station application by combining the proposed LB and HB element. By utilizing multiple folded-dipole antennas (MFDA), a LB element with a high out-of-band rejection level and low cross-band scattering is realized. The working principle of the MFDA is firstly explained in this paper based on the proposed transmission line model of the double folded-dipole antenna (DFDA). By introducing a meander line loop (MLL), rectangular loop (RL) and V-shaped strips (VSS), a novel filtering antenna with a high Roll-off rate (RoR) is realized to cover the HB. The working principle of the MLL is analyzed in detail in this paper by utilizing an equivalent circuit. To validate the performance of the proposed designs, an interleaved shared-aperture dual-band array antenna including one LB element and four HB elements is designed. The measured and simulated results demonstrate that the proposed designs maintain a good performance in the proposed dual-band array. Besides, to suppress the mutual coupling between the HB sub-arrays, eight shorted strips are introduced next to the HB elements. After introducing the shorted strips, the mutual couplings between the HB arrays can be effectively reduced to below -22 dB. All the simulations in this paper are completed by using the commercial electromagnetic simulation software Ansys HFSS.

II. DESIGN OF ANTENNA ELEMENTS

In this section, LB and HB antenna elements are presented for the design of the dual-band dual-polarized array antenna. The LB MFDA has a wide bandwidth, two upper radiation nulls, and innate EM transparent characteristics in HB. The HB element features wide bandwidth and a high RoR of 242.9 dB/GHz with two radiation nulls in LB.

A. LB Element

The configurations of the proposed MFDA are shown in Fig.1. The MFDA contains two Rogers RO4003 substrates with a thickness of 0.508 mm ($\varepsilon_r = 3.55$). As can be observed, the MFDA is printed on the upper layer of substrate 1. To
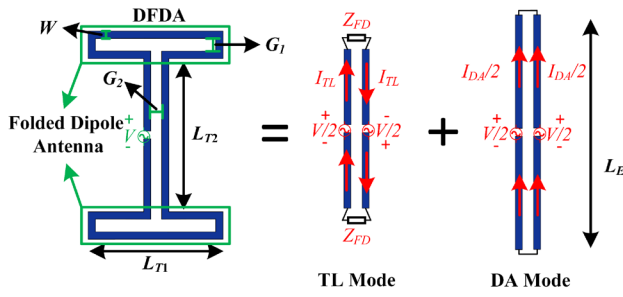
Fig. 3. Configuration and decomposition of DFDA.

enhance the out-of-band rejection level, four parasitic rectangular loops are placed under the MFDA. The configurations and dimensions of the baluns are given in Fig. 1(d). The radiator and the ground plane are connected by the feeding baluns. By using the above configuration, the proposed MFDA has the advantages of wide bandwidth, two upper radiation nulls, and EM transparent characteristics in HB. To have a deeper insight into the proposed antenna, the working principle of the MFDA is interpreted in the following paragraphs.

For ± 45° polarization feeding ports, the proposed MFDA can be assumed as a combination of two bended DFDA as illustrated in Fig. 2. Thus, to have a deeper insight into MFDA, the working principle of DFDA is analyzed first. As shown in Fig. 3, the currents on the DFDA can be decomposed into two distinct modes: a transmission line mode (TL Mode) and a dipole antenna mode (DA Mode).

For the TL Mode, the conductors are driven by two generators with equal magnitude ($V/2$) and 180° phase difference. The current on the conductors is I_{TL}. By dividing the TL Mode into two identical loaded transmission lines with length $L_{T2}/2$ at the central plane, the impedance of each part can be derived from:

$$Z_{TL2} = Z_c \frac{Z_{FD} + jZ_c\tan{(k\frac{L_{T2}}{2})}}{Z_c + jZ_{FD}\tan{(k\frac{L_{T2}}{2})}} \tag{1}$$

where Z_c is the characteristic impedance of two-wire transmission lines. Z_{FD} is the impedance of the folded-dipole antenna. k is the propagation constant, and L_{T2} is the length of the transmission line. Z_c can be calculated by substituting W, and $g = G_2$ into (2)-(4) [34]:

$$Z_c = 120\pi \frac{K(x)}{K(x')} \tag{2}$$

$$x^2 + x'^2 = 1 \tag{3}$$

$$x = \frac{g}{g + 2W} \tag{4}$$

where $K(x)$ is the complete elliptic function of the first kind. The impedance of the folded-dipole antenna [35] is:

$$Z_{FD} = \frac{4Z_{DA1}Z_{TL1}}{2Z_{DA1} + Z_{TL1}} \tag{5}$$

where Z_{TL1} is the impedances of its transmission line mode.

$$Z_{TL1} = jZ_c\tan{(k\frac{L_{T1}}{2})} \tag{6}$$

By substituting $l = L_{T1}$ into (7), the impedance of equivalent dipole antenna mode Z_{DA1} can be obtained [35].

$$Z_{DA} = \frac{R_{DA} + jX_{DA}}{sin^2(kl)} \tag{7}$$

where R_{DA1} and X_{DA1} can be expressed as:

$$R_{DA} = \frac{\eta}{2\pi} \begin{Bmatrix} C + \ln(kl) - C_i(kl) + \\ \frac{1}{2}sin(kl)[S_i(2kl) - 2S_i(kl)] + \\ \frac{1}{2}\cos{(kl)}\begin{bmatrix} C + \ln\left(k\frac{l}{2}\right) + C_i(2kl) \\ -2C_i(kl) \end{bmatrix} \end{Bmatrix} \tag{8}$$

$$X_{DA} = \frac{\eta}{4\pi} \begin{Bmatrix} 2S_i(kl) + \\ \cos(kl)\left[2S_i(kl) - S_i(2kl)\right] - \\ sin(kl)\left[2C_i(kl) - C_i(2kl) - C_i\left(2k\frac{a_E}{l}\right)\right] \end{Bmatrix} \tag{9}$$

where a_E represents the equivalent radius of the dipole and, it can be calculated by substituting $g = G_1$ into (9):

$$a_E = \sqrt[2]{\frac{W}{4}\left(\frac{g + W}{2} + \sqrt[2]{\left(\frac{g + W}{2}\right)^2 - \left(\frac{W}{4}\right)^2}\right)} \tag{10}$$

Therefore, the current I_{TL} can be calculated by using:

$$I_{TL} = \frac{V/2}{Z_{TL2}} \tag{11}$$

For the DA Mode, the conductors are driven by two identical generators with equal magnitude ($V/2$). It can be equivalent to a dipole antenna with equivalent radius (a_E) and equivalent length L_E. The equivalent length L_E can be obtained by using the method in [36]. The impedance of DA Mode Z_{DA2} can be calculated by substituting W, $l = L_E$, $g = G_2$ into equations (7)-(10). The current for the DA Mode is given by:
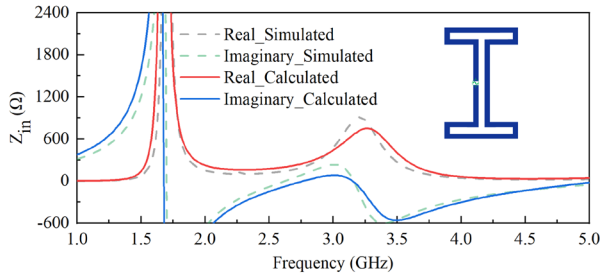
Fig. 4.   Calculated and simulated input impedances of DFDA without substrate.
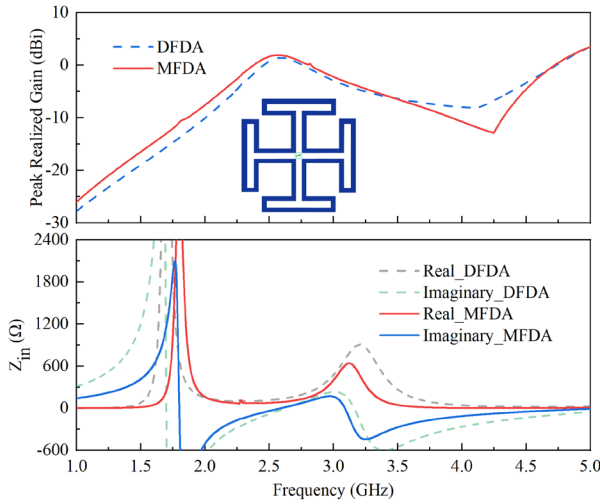

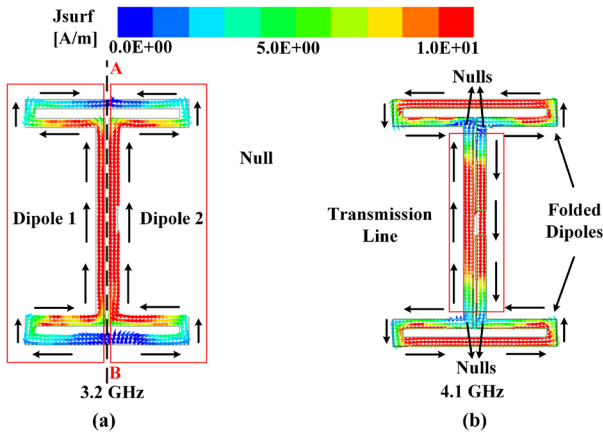Fig. 5. Simulated peak realized gains and input impedances of the DFDA and MFDA.

Fig. 6. Simulated current distributions of the DFDA at (a) 3.2 GHz and (b) 4.1 GHz.

$$I_{DA} = \frac{V/2}{Z_{DA2}} \tag{12}$$

Thus, the total current on the DFDA I_{IN} is given by:

$$I_{IN} = I_{TL} + \frac{I_{DA}}{2} = \frac{V(2Z_{DA2} + Z_{TL2})}{4Z_{DA2}Z_{TL2}} \tag{13}$$
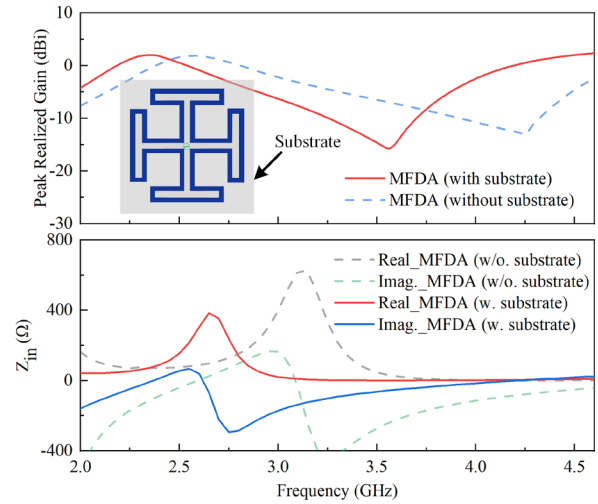
The impedance of DFDA is given by:

Fig. 7. Simulated peak realized gains and input impedances of the MFDA with and without substrate.

$$Z_{IN} = \frac{4Z_{DA2}Z_{TL2}}{2Z_{DA2} + Z_{TL2}} \tag{14}$$

Based on the analysis above, the input impedance of the DFDA is calculated by using Matlab. As shown in Fig. 4, the calculated results agree well with the simulated results. Thus, the proposed TL and DA model can be used to accurately analyze impedance characteristic of DFDA.

As shown in Fig. 5, a radiative resonant mode and radiation null appears at 3.2 GHz and 4.1 GHz, respectively. To understand the working principles of them, the simulated current distributions are given in Fig. 6. It can be seen from Fig. 6(a) that the DA mode plays a dominate role at 3.2 GHz in effective radiation. Owing to the currents flowing in the same direction on both sides, the symmetrical plane (A-B) can be equivalent to an open circuit, and the currents flow in the same direction on both sides. The current distribution of the DFDA in Fig. 6(b) demonstrates that the TL mode is the dominant mode at 4.1 GHz. At this frequency, the currents on the central part of the DFDA flow in opposite directions. It can be seen as a section of transmission line. The current distribution on the two folded dipoles show that they work under their 1st-order mode [37]. As mentioned in [37], the input resistance of the 1st-order mode of linear folded dipole is very large and close to infinite. So, they can be equivalent to open circuits. Therefore, no power will be radiated into the free space at this frequency. This can also be verified by the current distribution in Fig. 6(b). It can be seen that there are four current nulls at the inputs of the folded dipoles. All the power will be reflected back to the source at this frequency. Thus, a radiation null appears at this frequency. Then, by combining two bended DFDA, a MFDA is obtained. It can be seen in Fig. 5 that the resonant frequencies of the radiative mode and radiation null of the MFDA are almost same as the DFDA.

It is worth noting that the influences of the substrate on the DFDA and MFDA are not included in the calculation and
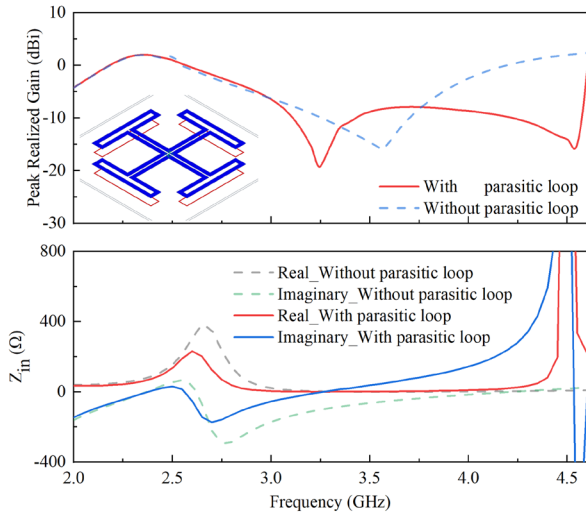
Fig. 8. Simulated peak realized gains and input impedances of the MFDA with and without parasitic loops.
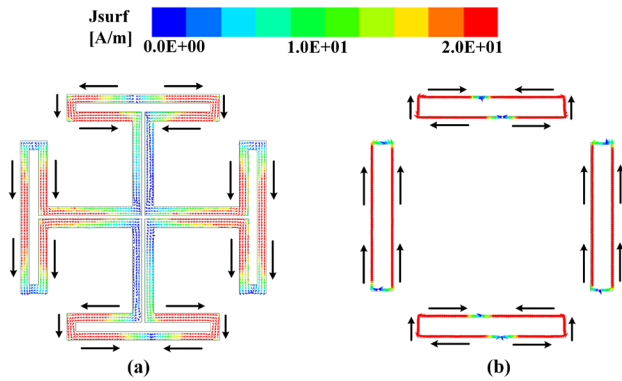

Fig. 9. Simulated current distributions of the antenna on (a) MFDA and (b) parasitic rectangular loops at 4.5 GHz.
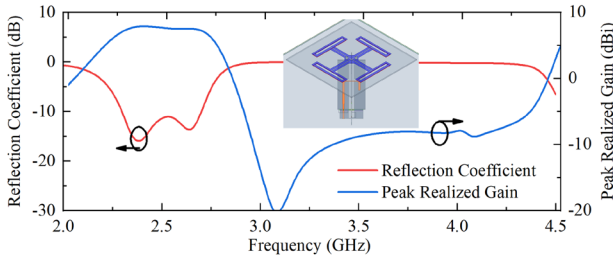

Fig. 10. Configuration and simulated results of the proposed LB element.

simulation presented above. To facilitate fabrication, a Rogers 4003 substrate with a thickness of 0.508mm is introduced to support the MFDA. As given in Fig. 7, the resonant mode and radiation null shift towards a lower frequency band after introducing the substrate.

In the presented antenna, four parasitic rectangular loops are placed under the MFDA to further enhance the out-of-band rejection level of the higher frequency band. As shown in Fig.8, the 1st radiation null shifts towards lower frequency after introducing the parasitic loops, and the input impedance of the radiative resonant mode is reduced. Furthermore, a new radiation null (2nd radiation null) is introduced at 4.5 GHz. To
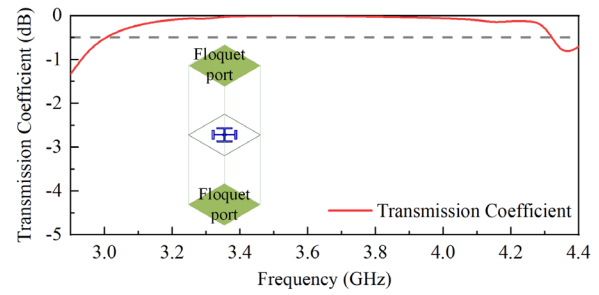

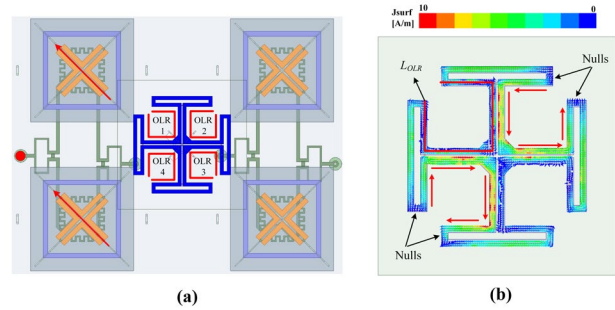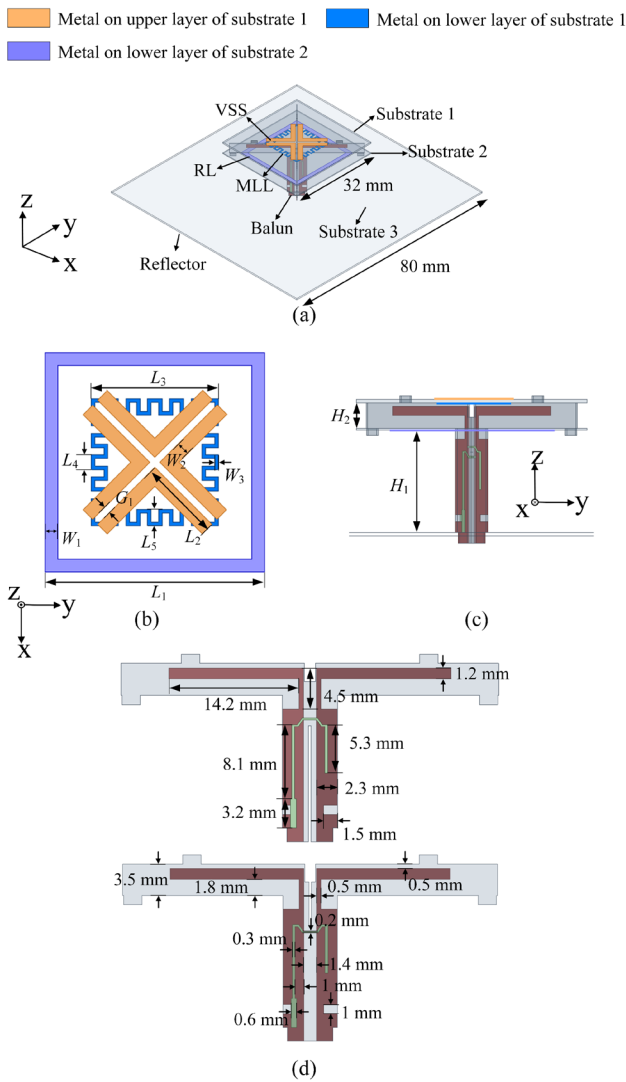Fig. 11. Simulated transmission coefficient of the proposed radiator.

Fig. 12. (a) Configuration of the dual-band array, and (b) simulated current distribution on the radiator at 3.6 GHz when the HB sub-array is excited.

interpret the working principle of the 2nd radiation null, the simulated current distribution of the antenna at 4.5 GHz is given in Fig. 9. It can be observed that the current distributions on the parasitic rectangular loops are opposite to the current distributions on the MFDA. Thus, the radiation power in the far-field zone is cancelled by each other. Due to all the power being reflected back to the source, a new radiation null is obtained at this frequency.

Then, by feeding the antenna using two orthogonal printed baluns, a $\pm 45°$ dual-polarization antenna with a compact size and upper out-of-band rejection is achieved. The simulated peak realized gain and reflection coefficient are shown in Fig. 10. The proposed antenna can cover the frequency range of 2.3 GHz -2.7 GHz. Besides, the out-of-band rejection level is higher than 16 dB.

Apart from the advantages mentioned above, the proposed antenna also has an electromagnetic transparent characteristic at higher frequency band. The simulated transmission coefficient of the LB radiator is shown in Fig. 11. It can be observed that the simulated transmission coefficient of the proposed radiator is higher than -0.5 dB from 3.0 GHz to 4.3 GHz. Due to the high transmission coefficient level, the proposed LB antenna has little influence on the radiation patterns of the HB antennas.

As shown in Fig. 12(a), the LB radiator has four open loop resonators (OLRs). Each OLR can be equivalent to a LC parallel resonance circuit, working as a bandpass surface, which is transparent to the wave radiated from the HB antenna. As shown in Fig. 12(b), when -45° polarized incident electromagnetic wave irradiates the LB radiator, the OLR 2 and 4 are excited and play an important role in transmitting the wave through them. Due to the symmetry of the radiator, it will be the same phenomenon that the OLR 1 and 3 will be

Fig. 14. Configuration and simulated results of the HB element.

Fig. 15. Evolution of the HB element.

Fig. 13. Configuration of the proposed HB antenna. (a) 3D view, (b) top view, (c) side view, and (d) Balun and dipole arms. Dimensions are L_1 = 24.2, L_2 = 8.9, L_3 = 22.8, L_4 = 1.6, L_5 = 1.8, W_1 = 1.4, W_2 = 1.5, W_3 = 0.4, G_1 = 0.8, H_1 = 14.2, H_2 = 3.5. (unit: millimeter).

excited when +45° polarized incident electromagnetic wave irradiates on the LB radiator. As a result, HB electromagnetic wave can be transmitted through the LB radiator without being affected. Therefore, the LB antenna can be seen as an electromagnetic transparent antenna for the HB antennas. The resonant frequency of the OLRs (central frequency of the EM transparent band) can be calculated by using:

$$f_{OLR} \approx \frac{c}{2L_{OLR}} \qquad (15)$$

where c is the speed of the light in free space, L_{OLR} is the length of the OLR.

In this sub-section, the DFDA is firstly analyzed by using TL and DA modes. The calculated input impedance of the DFDA agrees well with the simulated one. Based on the analysis, the working mode of the DFDA can be divided into DA mode and TL mode. Under the TL mode, the DFDA will transmit the electromagnetic wave into free space. Under the
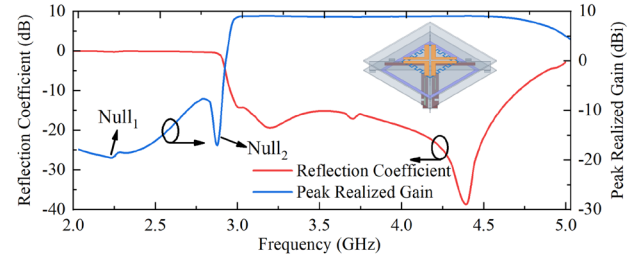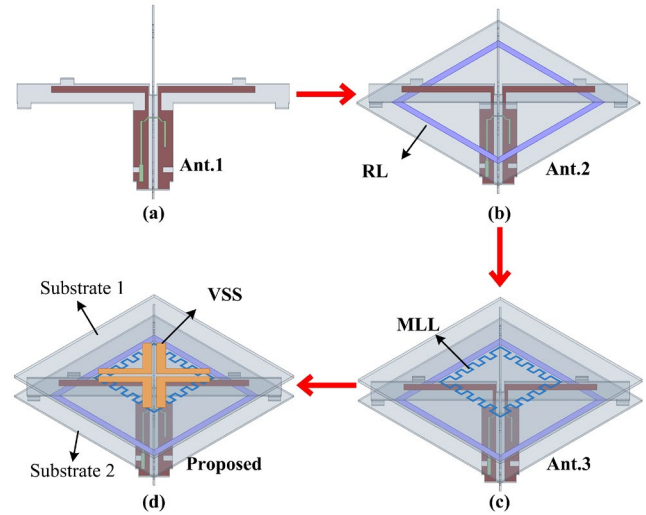
TL mode, all the power will be reflected back to the source. Therefore, by combining two bended DFDA and introducing four parasitic loops, a LB antenna with compact size and good performance can be obtained. Moreover, the proposed antenna has little influence on the radiation patterns of the HB array owing to the EM transparent characteristic. These are very important advantages in the design of dual-band dual-polarized base station array antenna.

B. HB Element

Having a HB element with a good out-of-band suppression level in lower frequency band is critical in the design of a dual-band base station array antenna with low couplings. In this section, a HB element with a high suppression level and sharp cut-off in the lower frequency band is achieved by using meander line loop (MLL), rectangular loop (RL) and V-shaped strips (VSS).

The configurations and dimensions of the proposed HB antenna are given in Fig. 13. It can be seen that all conductors of the proposed HB element are printed on three Rogers RO4003 substrates with a thickness of 0.508 mm, 0.305 mm, and 0.508mm, respectively. The VSS and MLL are printed on the upper and lower layer of substrate 1. The RL is printed on the lower layer of the Substrate 2. The dipole arms of this antenna are vertically printed and connected to the baluns.

The simulated peak realized gain and reflection coefficient are shown in Fig. 14. It can be seen that the proposed HB element has a wide impedance bandwidth of 42.5% (3.0- 4.62
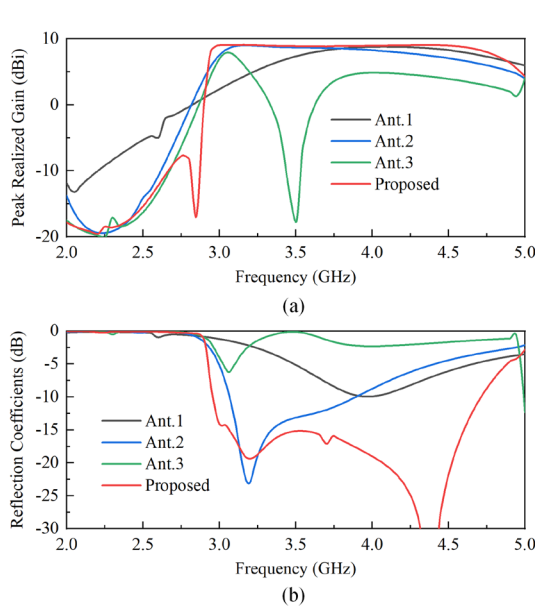
Fig. 16. Simulated normalized peak realized gain and reflection coefficients of the proposed HB element and reference antennas.

GHz), a stable peak realized gain of 8.9 dBi and a good out-of-band rejection level of 17 dB. Besides, the proposed antenna obtains a high Roll-off rate (*RoR*) of 242.9 dB/GHz ($f_{20\ dB}$ is 2.87 GHz, $f_{3\ dB}$ is 2.94 GHz), which is crucial in the design of multi-band array antenna with low frequency ratio. The *RoR* is calculated by using [38]:

$$RoR = \frac{20 - 3}{|f_{20\ dB} - f_{3\ dB}|} \tag{16}$$

where the frequency $f_{3\ dB}$ and $f_{20\ dB}$ are the frequencies where the average peak realized gain drops by 3 dB and 20 dB, respectively.

To better demonstrate the working principle of the proposed HB element, three reference antennas are given in Fig. 15. The Ant.1 is a vertically printed crossed dipole antenna. By introducing a RL under the arms of the Ant.1, 1st radiation null and a new resonant mode can be obtained to suppress the out-of-band radiation and expand the impedance bandwidth [39]. To further enhance the roll-off rate, a MLL is placed above the arms of the crossed dipoles in Ant.2. After introducing the MLL, a new radiation null appears at the in-band of the antenna. Finally, four VSS are introduced above the MLL to shift the 2nd radiation null towards lower frequency band.

Fig. 16 shows the simulated results of the reference antennas and proposed HB element. It can be observed that the out-of-band rejection of the Ant.1 can be effectively developed by introducing the RL. Besides, the bandwidth is increased due to the new resonant mode. Then, by introducing a MLL above the dipole arms, the 2nd radiation null is realized at 3.5 GHz.

To interpret the working principle of the 2nd radiation null, the equivalent circuit of MLL is given in Fig. 17. For the -45° polarization, the MLL can be divided into two identical parts (Part 1 and Part 2). Each part has two meander line (ML)
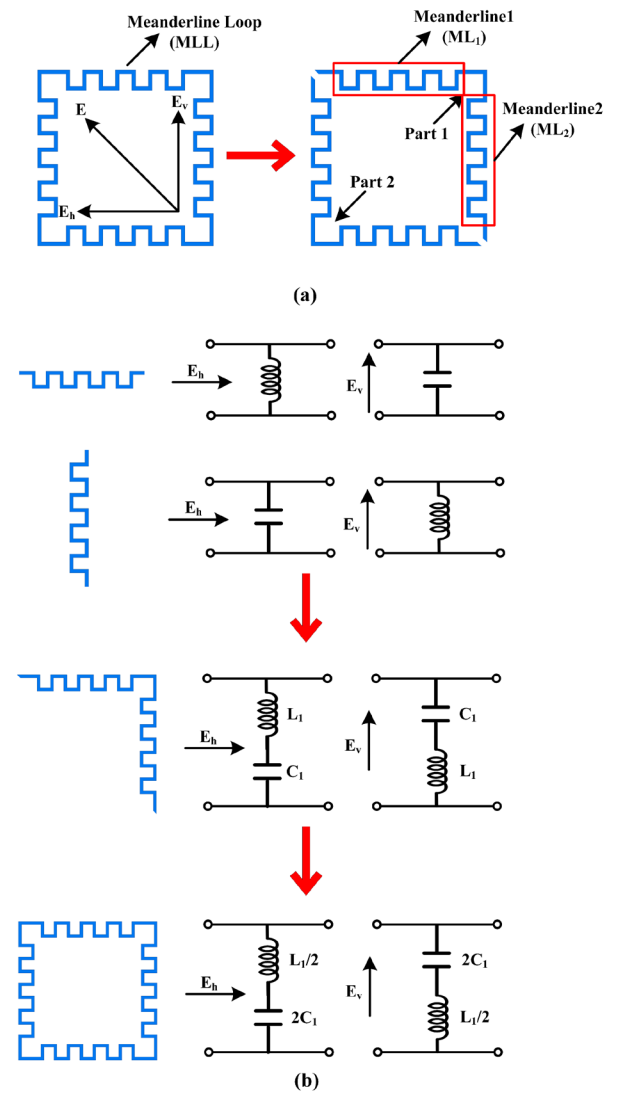
Fig. 17. Equivalent circuits of the MLL.

elements. One is horizontally printed; another is vertically printed. For horizontal electric field (E_h), ML_1 can be equivalent to a shunt inductance over an equivalent transmission line and ML_2 can be equivalent to a shunt capacitance. For vertical electric field (E_v), ML_1 will acts like a shunt capacitance and ML_2 will acts like a shunt inductance [40]. Therefore, for the horizontal and vertical electric field, Part 1 can be equivalent to a series *L-C* resonator. The MLL acts like a band-stop filter. The resonant frequency of the MLL can be calculated by employing:

$$f_{null} = \frac{1}{2\pi\sqrt{L_1 C_1}} \tag{17}$$

To shift the 2nd radiation null out of the operating band of the HB element, four parasitic VSSs are introduced above the MLL. It can be observed from Fig. 16 that the 2nd radiation null is moved from 3.5 GHz to 2.9 GHz without increasing the aperture of the antenna after introducing the VSSs. Besides, the *RoR* increases from 45.9 dB/GHz to 242.9 dB/GHz.

This article has been accepted for publication in IEEE Transactions on Antennas and Propagation. This is the author's version which has not been fully edited and content may change prior to final publication. Citation information: DOI 10.1109/TAP.2022.3209177

> REPLACE THIS LINE WITH YOUR PAPER IDENTIFICATION NUMBER (DOUBLE-CLICK HERE TO EDIT) <   8
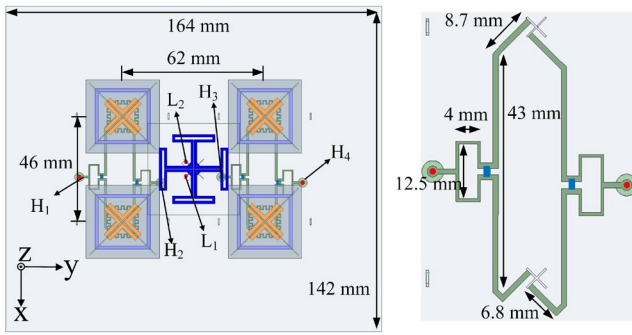

Fig. 18. Configuration of the dual-band dual-polarized array antenna.
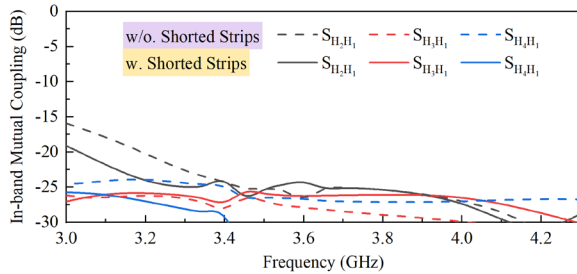

Fig. 19. Simulated isolations of the HB sub-arrays with and without shorted strips.

Overall, in this sub-section, a novel HB element with high *RoR* is proposed by combining the RL, MLL, and VSS. Firstly, a RL is placed under the arms of the crossed dipoles to obtain the 1st radiation null and excite a new resonant mode. Then, to enhance the *RoR* and out-of-band rejection level, a MLL is printed above the dipole arms. The working principle of the MLL is then analyzed. By introducing four VSSs, the 2nd radiation null can be shifted towards the lower frequency band. As a result, a HB element with wide impedance bandwidth and a high roll-off rate is achieved in this work.

III. DUAL-BAND DUAL-POLARIZED ARRAY

Based on the LB and HB elements designed above, a dual-band dual-polarized array antenna is realized in this section. As shown in Fig. 18, the size of the ground plane is 164 mm × 142mm. The LB element is placed in the center of the ground plane and above the HB elements. The four HB elements are divided into two columns. Elements in each column are fed by two Wilkinson power dividers. The distances between the elements along the x-axis and y-axis are 46 mm and 62 mm, respectively.

It should be noted that eight shorted strips are introduced to reduce the coupling between the input ports of the HB
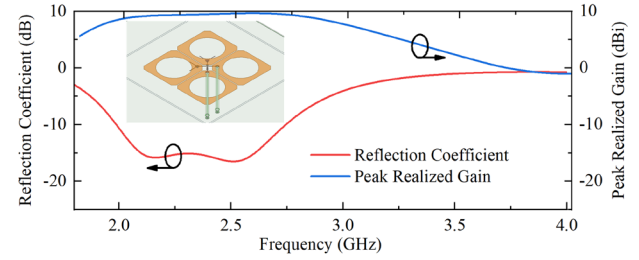

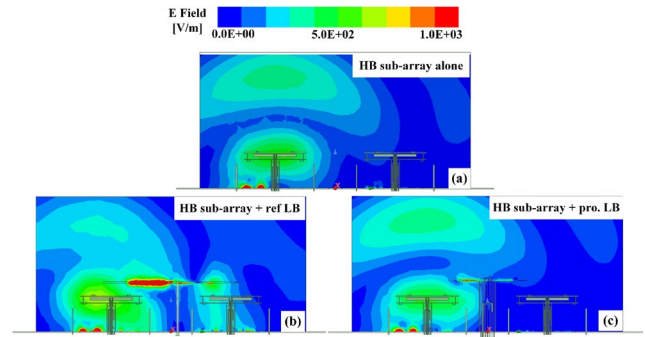Fig. 20. Configuration and simulated results of the reference LB element.

Fig. 21. Simulated E-Field distributions of the HB sub-array (port H_1 excited) at 3.6 GHz under different configurations. (a) HB sub-array alone, (b) HB sub-array + reference LB element, and (c) HB sub-array + MFDA.
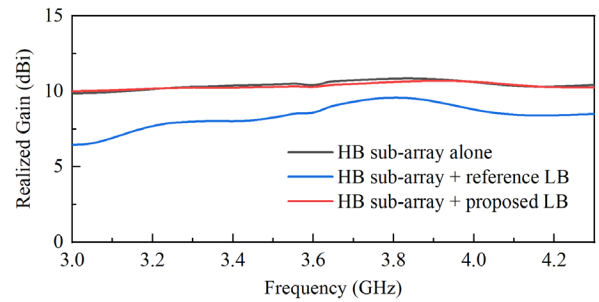
Fig. 22. Simulated peak realized gains of the HB sub-array (port H_1 excited) under different configurations.

elements. Fig. 19 shows the simulated reflection coefficients of the proposed HB array with and without shorted strips. As can be seen, the isolation between port H_1 and port H_2 increase from 15 dB to 19 dB after introducing the shorted strips. It demonstrates that the shorted strips play an important role in reducing the mutual couplings between the HB sub-arrays.

To verify the performance of the proposed antenna, a reference dual-band array antenna is designed by using the most common crossed dipole elements. The configurations of these two dual-band array antennas are the same except for the LB elements. The configuration and simulated results of the reference LB element are shown in Fig. 20. The E-field distributions of the HB sub-array are given in Fig. 21. It can be observed that the HB sub-array is severely blocked by the reference LB antenna when using the ordinary dual-polarized crossed dipole antenna. The E-field of the HB sub-array is disturbed and reflected. As a result, the radiation performance of the HB sub-array will be seriously distorted. The simulated peak realized gains of the HB sub-array under different
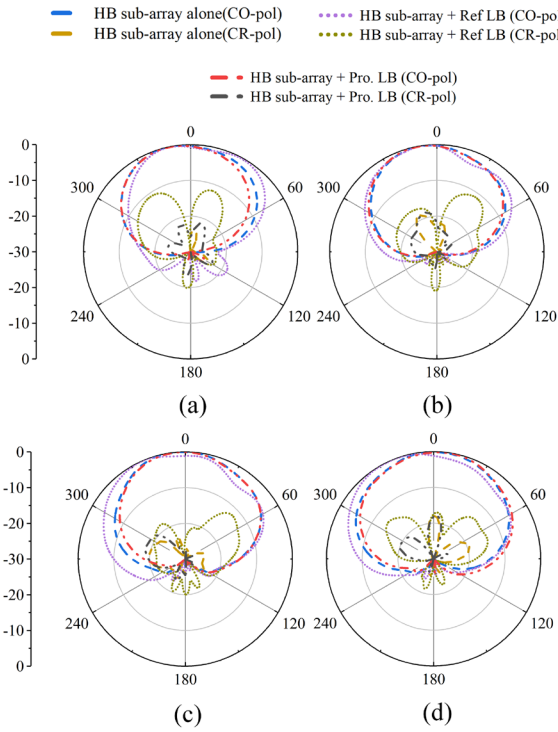
Fig. 23. Simulated normalized radiation patterns of the HB sub-array (port H_1 excited) in the horizontal plane under different configurations at (a) 3.0 GHz, (b) 3.6 GHz, (c) 4.0 GHz, and (d) 4.3 GHz.
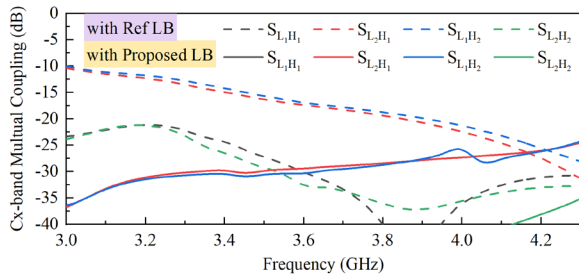

Fig. 24. Simulated cross-band coupling of the proposed array antenna and the reference array antenna.

Fig. 25. The fabricated prototype of the dual-band array antenna.
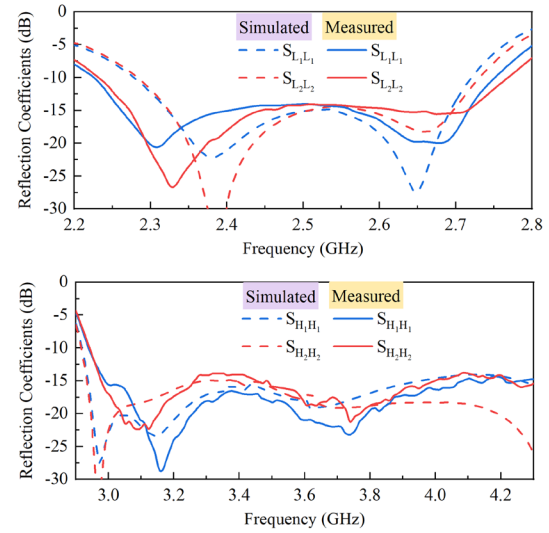
Fig. 26. Measured and simulated reflection coefficients of the dual-band array antenna.

configurations are shown in Fig. 22. It can be seen the peak realized gain of the HB sub-array drops 3.6 dB at 3 GHz after introducing the reference LB element, which is unacceptable in dual-band base station application. However, by comparing the E-field distributions in Fig. 21(a) and (c), it is not difficult to find that the proposed LB element has little influence on the radiation performance of the HB sub-array and it can be seen as an EM transparent antenna at this frequency. Besides, as depicted in Fig. 22, the peak realized gain of the HB sub-array keeps almost unchanged after introducing the proposed LB element. The max gain difference is only 0.2 dB.

The comparison between the radiation patterns of the higher band sub-array (without LB element, with reference LB element, and with proposed LB element) is given in Fig. 23. As depicted, the reference LB element has a great influence on the radiation patterns of the HB sub-array. When using the ordinary LB element, both co-polarized and cross-polarized radiation patterns of the HB sub-array are deteriorated.

However, by replacing it with the proposed LB element, the radiation patterns of the HB sub-array remain almost unchanged. This is highly desirable for nowadays base station applications.

Besides, due to the good filtering performance of the proposed LB element, the cross-band coupling of the proposed dual-band array antenna is much lower than the reference one, as depicted in Fig. 24. The simulated isolations between the HB sub-array and the reference LB element are higher than 10 dB from 3 GHz to 4.3 GHz. However, in the proposed dual-band array antenna, the isolations between the HB sub-array and the proposed LB element are higher than 24 dB within the same frequency band, which shows a significant improvement in the array design.

In this section, based on the proposed LB element and HB element, a novel dual-band dual-polarized base station array antenna is achieved. To validate the advantages of the proposed antenna, a reference dual-band array antenna is designed. It is worth noting that the only difference between these two dual-band array antennas is the structure of the LB element. Simulated results demonstrate the proposed LB element has little influence on the radiation performance of the HB array. Furthermore, the proposed dual-band array antenna shows a significant improvement in cross-band isolation.

Fig. 27. Measured and simulated mutual couplings of the dual-band array antenna.

Fig. 28. Measured and simulated realized gain of the dual-band array antenna.

Fig. 29. Measured and simulated normalized radiation patterns of the LB element in the horizontal plane at (a) 2.3 GHz, and (b) 2.7 GHz.
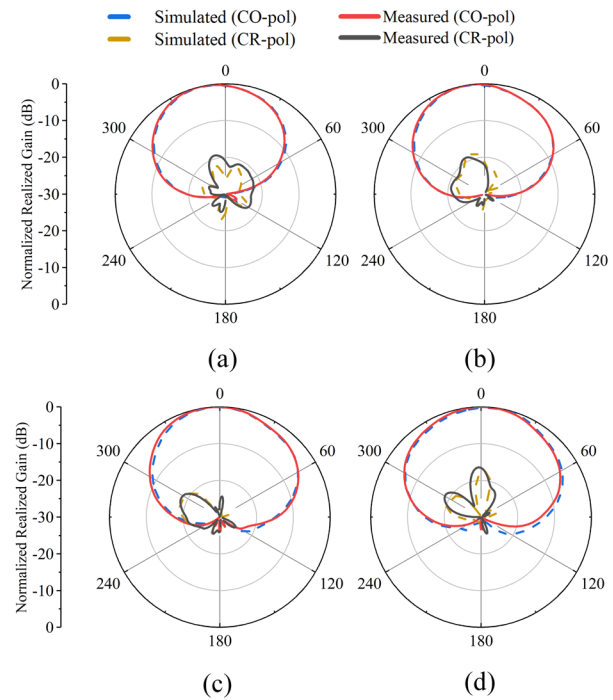
Fig. 30. Measured and simulated normalized radiation patterns of the HB sub-array in the horizontal plane at (a) 3.0 GHz, (b) 3.6 GHz, (c) 4.0 GHz, and (d) 4.3 GHz.

IV. RESULTS AND DISCUSSION

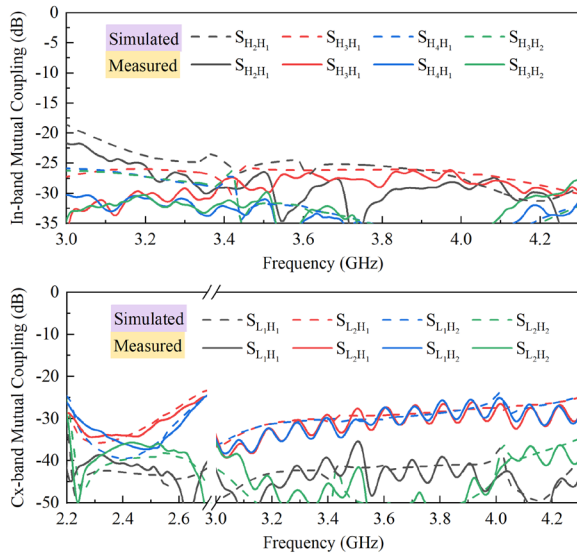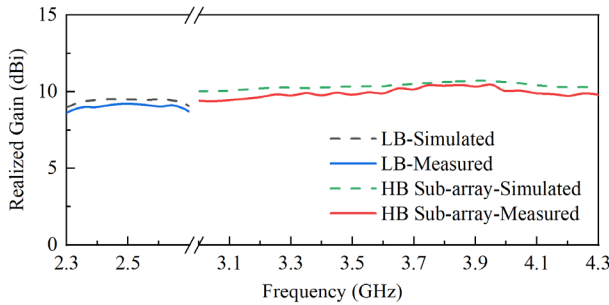For verification, a prototype of the proposed dual-band dual-polarized array antenna is fabricated as shown in Fig.25. The measured S-parameters are obtained by using the R&S®ZVL vector network analyzer. The far-field results are obtained in the anechoic chamber at University of Kent. Fig. 26 shows the measured and simulated reflection coefficients of the LB element and HB array in the dual-band array. According to the measured results, the proposed LB element has an impedance bandwidth of 18.8% (2.26 GHz-2.73 GHz) with a reflection coefficient < -14 dB. For the HB sub-array, the measured and simulated results are in reasonable agreement with each other. The measured results indicate that the proposed HB sub-array realize a wide bandwidth of 36% (2.98 GHz- 4.3 GHz) for reflection coefficients lower than -14 dB.

Fig. 27 exhibits the measured and simulated in-band and cross-band mutual couplings of the proposed dual-band array antenna. It can be observed from the measured results that the in-band isolations between the port H_1 and port H_2 are higher than 22 dB. The isolations between other ports of the HB sub-arrays are higher than 25 dB. Due to the good filtering performance of the proposed LB and HB element, the cross-

band mutual couplings between the input ports of the LB element and HB sub-arrays are all higher than 25 dB.

The measured and simulated broadside realized gains of the proposed dual-band array antenna are shown in Fig. 28. For the LB element, an average measured realized gain of 8.9 dBi is achieved within the operating band. It is slightly lower than the simulated value of 9.2 dBi because of the loss of the cables and test environment. For the HB sub-array, the measured realized gains distribute between 9.4 dBi and 10.5 dBi while the simulated one is all within the range of 10 dBi -10.7 dBi. The ripples in the operating band, as well as the slight gain variation between the measured and simulated curves, can be attributed to the loss of the test equipment and fabrication error.

The measured and simulated normalized radiation patterns of the LB element and HB sub-array in the horizontal plane at

TABLE I
COMPARISON OF THE PREVIOUSLY PRESENTED DUAL-BAND DUAL-POLARIZED ARRAY ANTENNAS

Ref.	Elements Arrangement	HB (GHz); $|S_{11}|$ (dB)	LB (GHz); $|S_{11}|$ (dB)	Freq. Ratio	Gain of LB element (dBi)	Cx-band Iso. (dB)	In-band Iso. (dB)	HB Elements Spacing (λ_{HL})
[20]	2×2 HB above LB	3.5-4.9 (33%); -14	0.69-0.96 (33%); -10	5.09	8.7 ± 1	24	21	0.73 × 0.73
[21]	2×2 HB above LB	3.4-3.7 (8%); -10	0.69-0.96 (33%); -10	4.3	7.4 ± 0.3	32	20	0.54 × 0.54
[23]	Coplanar 2×2 HB and LB	3.3-3.8 (14%); -14	0.69-0.96 (33%); -14	4.3	8.7 ± 0.6	29	25	0.92 × 0.92
[24]	2×2 HB under LB	3.4-3.8 (11%); -14	0.69-0.96 (33%); -14	4.36	6.8 ± /	/	/	0.51 × 0.68
[25]	2×2 HB under LB	1.7-2.7 (46%); -14	0.69-0.96 (33%); -14	2.7	7.6 ± 0.6	19	19	/
[26]	2×2 HB under LB	1.71-2.28 (28%); -14	0.82-1.0 (20%); -10	2.19	6.5 ± 0.5	/	/	0.57 × 0.86
[27]	2×2 HB under LB	3.3-3.8 (14%); -11	1.71-2.17 (24%); -12	1.8	7.9 ± 0.5	20	20	0.5 × 0.66
[29]	2×2 HB under LB	3.3-3.8 (14%); -12	1.8-2.7 (40%); -10	1.58	8.6 ± 1.3	20	20	0.47 × 0.69
[30]	A LB stacked on a HB	3.3-3.8 (14%); -14	2.3-2.7 (16%); -14	1.42	9.1 ± 0.3	/	/	/
This Work	**2×2 HB under LB**	**3.0-4.3 (36%); -14**	**2.26-2.73 (19%); -14**	**1.46**	**8.9 ± 0.3**	**25**	**22**	**0.46 × 0.62**

* λ_{HL}, and λ_{LL} are the wavelength at the lowest operating frequency in free space of higher band and lower band, respectively. Iso. represents isolation.

different frequencies are shown in Fig. 29 and Fig. 30, respectively. As can be observed, the measured results are in good agreement with the simulated results. The measured cross-polarization levels of the LB element and HB array are 20 dB and 21 dB lower than their co-polarization levels in broadside.

The comparisons between the proposed antenna and recently published dual-band dual-polarized array antennas are shown in Table I. By introducing FSS structure [20],[21] and etching the HB elements in the dipole arms of the LB element [23], three dual-band arrays with high cross-band isolations are developed. However, the frequency ratios of these antennas are larger than 4.3. In [24] and [25], two interleaved shared-aperture dual-band array antennas are realized by introducing branches on the radiator of LB element. However, the frequency ratios of these two dual-band array antennas are near twice of the proposed antenna. Four dual-band array antennas with frequency ratios smaller than 2 are developed in [27], [29]-[31]. Although the LB element in [27], [29], and [30] obtain a wider impedance bandwidth than the proposed one, the wave-transparent band of them are much narrower than our work. Besides, the proposed dual-band array antenna realizes a smaller frequency ratio, a higher gain, and a higher isolation than the designs in [27] and [30]. LB element in [31] achieves a high realized gain of 9.1 dBi, however, the impedance bandwidths of both LB and HB in this design are narrower than our work.

V. CONCLUSION

Two new methods are proposed in this paper to design the LB and HB elements in the dual-band dual-polarized array antenna. Based on the proposed method, a novel low scattering low-pass LB element and a novel high *RoR* high-

pass HB element are able to realize. By combining these two high-performance elements and introducing eight shorted strips, a novel shared-aperture dual-band dual-polarized array antenna with wide impedance bandwidths, high in-band and cross-band isolation, and low cross-band scattering can be realized. The measured results show that the proposed array antenna works at 2.26- 2.73 GHz and 2.98- 4.3 GHz with reflection coefficients lower than -14 dB. The in-band and cross-band isolations of the proposed array antenna are higher than 22dB and 25 dB, respectively. Such a high-performance dual-band dual-polarized array antenna is a good candidate for nowadays base station applications.

REFERENCES

[1] H. Zhai, L. Xi, Y. Zang and L. Li, "A low-profile dual-polarized high-isolation MIMO antenna arrays for wideband base-station applications," *IEEE Trans. Antennas Propag.*, vol. 66, no. 1, pp. 191-202, Jan. 2018.

[2] J. Yin, Y. Jia, S. Yang and H. Zhai, "Design of a composite decoupling structure for dual-band dual-polarized base station arrays," *IEEE Antennas Wireless Propag. Lett.*, early access, doi: 10.1109/LAWP.2022.3170081.

[3] Y. He, Z. Pan, X. Cheng, Y. He, J. Qiao and M. M. Tentzeris, "A novel dual-band, dual-polarized, miniaturized and low-profile base station antenna," *IEEE Trans. Antennas Propag.*, vol. 63, no. 12, pp. 5399-5408, Dec. 2015.

[4] H. Huang, Y. Liu and S. Gong, "A novel dual-broadband and dual-polarized antenna for 2G/3G/LTE base stations," *IEEE Trans. Antennas Propag.*, vol. 64, no. 9, pp. 4113-4118, Sept. 2016.

[5] B. Liu, Y. Da, X. Chen and A. A. Kishk, "Hybrid decoupling structure based on neutralization and partition schemes for compact large-scale base station arrays," *IEEE Antennas Wireless Propag. Lett.*, vol. 21, no. 2, pp. 267-271, Feb. 2022.

[6] M. Li, Q. Li, B. Wang, C. Zhou and S. Cheung, "A miniaturized dual-band base station array antenna using band notch dipole antenna elements and AMC reflectors," *IEEE Trans. Antennas Propag.*, vol. 66, no. 6, pp. 3189-3194, June 2018.

This article has been accepted for publication in IEEE Transactions on Antennas and Propagation. This is the author's version which has not been fully edited and content may change prior to final publication. Citation information: DOI 10.1109/TAP.2022.3209177

> REPLACE THIS LINE WITH YOUR PAPER IDENTIFICATION NUMBER (DOUBLE-CLICK HERE TO EDIT) < 12

[7] Y. Zhang, X. Y. Zhang, L. Ye and Y. Pan, "Dual-band base station array using filtering antenna elements for mutual coupling suppression," *IEEE Trans. Antennas Propag.*, vol. 64, no. 8, pp. 3423-3430, Aug. 2016.

[8] M. Li, R. Wang, J. M. Yasir and L. Jiang, "A miniaturized dual-band dual-polarized band-notched slot antenna array with high isolation for base station applications," *IEEE Trans. Antennas Propag.*, vol. 68, no. 2, pp. 795-804, Feb. 2020.

[9] W. Duan, Y. F. Cao, Y. -M. Pan, Z. X. Chen and X. Y. Zhang, "Compact dual-band dual-polarized base-station antenna array with a small frequency ratio using filtering elements," *IEEE Access.*, vol. 7, pp. 127800-127808, 2019.

[10] X. Zhang, D. Xue, L. Ye, Y. Pan and Y. Zhang, "Compact dual-band dual-polarized interleaved two-beam array with stable radiation pattern Bbased on filtering elements," *IEEE Trans. Antennas Propag.*, vol. 65, no. 9, pp. 4566-4575, Sept. 2017.

[11] X. Liu et al., "A compact dual-polarized filtering antenna with steep cut-off for base-station applications," *IEEE Trans. Antennas Propag.*, early access, doi: 10.1109/TAP.2022.3161280.

[12] C-X Mao, S. Gao, Y. Wang, Q. Luo, and Q-X. Chu, "A shared-aperture dual-Band dual-polarized filtering-antenna-array with improved frequency response," *IEEE Trans. Antennas Propag.*, vol. 65, no. 4, pp. 1836–1844, Apr. 2017.

[13] Y. Zhang, S. Zhang, J. Li and G. F. Pedersen, "A transmission-line-based decoupling method for MIMO antenna arrays," *IEEE Trans. Antennas Propag.*, vol. 67, no. 5, pp. 3117-3131, May 2019.

[14] Y. Zhang, S. Zhang, J. Li and G. F. Pedersen, "A wavetrap-based decoupling technique for 45° polarized MIMO antenna arrays," *IEEE Trans. Antennas Propag.*, vol. 68, no. 3, pp. 2148-2157, March 2020.

[15] H. Lin, W. Yu, F. Deng, B. Liao and R. Tang, "A compact wideband dual-polarized base station antenna using asymmetric dipole," *IEEE Open J. Antennas Propag.*, vol. 3, pp. 189-195, 2022.

[16] K. Wu, C. Wei, X. Mei and Z. Zhang, "Array-antenna decoupling surface," *IEEE Trans. Antennas Propag.*, vol. 65, no. 12, pp. 6728-6738, Dec. 2017.

[17] C. Wei, Z. -Y. Zhang and K. -L. Wu, "Phase compensation for decoupling of large-scale staggered dual-polarized dipole array antennas," *IEEE Trans. Antennas Propag.*, vol. 68, no. 4, pp. 2822-2831, April 2020.

[18] D. He, Y. Chen and S. Yang, "A low-profile triple-band shared-aperture antenna array for 5G base station applications," *IEEE Trans. Antennas Propag.*, vol. 70, no. 4, pp. 2732-2739, April 2022.

[19] Y. Chen, J. Zhao and S. Yang, "A novel stacked antenna configuration and its applications in dual-band shared-aperture base station antenna array designs," *IEEE Trans. Antennas Propag.*, vol. 67, no. 12, pp. 7234-7241, Dec. 2019.

[20] Y. Zhu, Y. Chen and S. Yang, "Decoupling and low-profile design of dual-band dual-polarized base station antennas using frequency-selective surface," *IEEE Trans. Antennas Propag.*, vol. 67, no. 8, pp. 5272-5281, Aug. 2019.

[21] Y. F. Cao, X. Y. Zhang and Q. Xue, "Compact shared-aperture dual-band dual-polarized array using filtering slot antenna and dual-function metasurface," *IEEE Trans. Antennas Propag.*, vol. 70, no. 2, pp. 1120-1131, Feb. 2022.

[22] Y. Zhu, Y. Chen and S. Yang, "Cross-band mutual coupling reduction in dual-band base-station antennas with a novel grid frequency selective surface," *IEEE Trans. Antennas Propag.*, vol. 69, no. 12, pp. 8991-8996, Dec. 2021.

[23] Y. Li and Q. -X. Chu, "Coplanar dual-band base station antenna array using concept of cavity-backed antennas," *IEEE Trans. Antennas Propag.*, vol. 69, no. 11, pp. 7343-7354, Nov. 2021.

[24] W. Niu, B. Sun, G. Zhou and Z. Lan, "Dual-band aperture shared antenna array with decreased radiation pattern distortion," *IEEE Trans. Antennas Propag.*, early access, doi: 10.1109/TAP.2022.3161267.

[25] Y. He, W. Huang, Z. He, L. Zhang, X. Gao and Z. Zeng, "A novel cross-band decoupled shared-aperture base station antenna array unit for 5G mobile communications," *IEEE Open J. Antennas Propag.*, vol. 3, pp. 583-593, 2022.

[26] H. -H. Sun, C. Ding, H. Zhu, B. Jones and Y. J. Guo, "Suppression of cross-band scattering in multiband antenna arrays," *IEEE Trans. Antennas Propag.*, vol. 67, no. 4, pp. 2379-2389, April 2019.

[27] S. J. Yang, R. Ma and X. Y. Zhang, "Self-decoupled dual-band dual-polarized aperture-shared antenna array," *IEEE Trans. Antennas Propag.*, vol. 70, no. 6, pp. 4890-4895, June 2022.

[28] S. J. Yang, Y. Yang and X. Y. Zhang, "Low scattering element-based aperture-shared array for multiband base stations," *IEEE Trans. Antennas Propag.*, vol. 69, no. 12, pp. 8315-8324, Dec. 2021.

[29] H. -H. Sun, H. Zhu, C. Ding, B. Jones and Y. J. Guo, "Scattering suppression in a 4G and 5G base station antenna array using spiral chokes," *IEEE Antennas Wireless Propag. Lett.*, vol. 19, no. 10, pp. 1818-1822, Oct. 2020.

[30] D. He, Q. Yu, Y. Chen and S. Yang, "Dual-band shared-aperture base station antenna array with electromagnetic transparent antenna elements," *IEEE Trans. Antennas Propag.*, vol. 69, no. 9, pp. 5596-5606, Sept. 2021.

[31] S. J. Yang and X. Y. Zhang, "Frequency selective surface-based dual-band dual-polarized high-gain antenna," *IEEE Trans. Antennas Propag.*, vol. 70, no. 3, pp. 1663-1671, March 2022.

[32] X. Lu, Y. Chen, S. Guo and S. Yang, "An electromagnetic-transparent cascade comb dipole antenna for multi-band shared-aperture base station antenna array," *IEEE Trans. Antennas Propag.*, vol. 70, no. 4, pp. 2750-2759, April 2022.

[33] Y. Qin, R. Li, Q. Xue, X. Zhang and Y. Cui, "Aperture-shared dual-band antennas with partially reflecting surfaces for base-station applications," *IEEE Trans. Antennas Propag.*, vol. 70, no. 5, pp. 3195-3207, May 2022.

[34] R. Lampe, "Design formulas for an asymmetric coplanar strip folded dipole," *IEEE Trans. Antennas Propag.*, vol. 33, no. 9, pp. 1028-1031, Sep. 1985.

[35] C. A. Balanis, *Antenna theory analysis and design*, 3rd ed. New York, U.S.: Willey, 2005.

[36] T. Endo, Y. Sunahara, S. Satoh, and T. Katagi, "Resonant frequency and radiation efficiency of meander line antennas," *Electronics and Communications in Japan, Part 2 (Electronics)*, vol. 83, pp. 52-58, 2000.

[37] W. Hu et al., "Compact wideband folded dipole antenna with multi-resonant modes," *IEEE Trans. Antennas Propag.*, vol. 67, no. 11, pp. 6789-6799, Nov. 2019.

[38] F. Chen, R. Li, J. Qiu and Q. Chu, "Sharp-rejection wideband bandstop filter using stepped impedance resonators," *IEEE Trans. Compon., Packag., Manuf. Technol.*, vol. 7, no. 3, pp. 444–449, Mar. 2017.

[39] C. F. Ding, X. Y. Zhang, Y. Zhang, Y. M. Pan and Q. Xue, "Compact broadband dual-polarized filtering dipole antenna with high selectivity for base-station applications," *IEEE Trans. Antennas Propag.*, vol. 66, no. 11, pp. 5747–5756, Nov. 2018.

[40] B. A. Munk, *Frequency selective surfaces*. New York: Wiley, 2000.

Xuekang Liu (Graduate Student Member, IEEE) received the M.S. degree (outstanding academic achievement) in electromagnetic field and microwave technology from Xidian University, Xi'an, China, in 2020. He is currently pursuing the Ph.D. degree with the School of Engineering, University of Kent, Canterbury, UK.

Mr. Liu was a recipient of the Best Student Paper Award (2nd Prize) from the 17th International Workshop on Antenna Technology (iWAT 2022, Dublin). His current research interests include multi-band base station antennas, filtering antennas, microstrip antennas, circularly polarized antennas, terminal antennas and omnidirectional antennas.

Steven Gao (Fellow, IEEE) received the PhD from Shanghai University, China.

He is a Professor at Department of Electronic Engineering, Chinese University of Hong Kong. Prior to this, he was a Chair Professor at the University of Kent, UK for nearly 10 years. His research covers smart antennas, phased arrays, MIMO, reconfigurable antennas,

broadband/multiband antennas, satellite antennas, RF/microwave/mm-wave/THz circuits, mobile communications, satellite communications, UWB radars, synthetic-aperture radars, sensors, IOT and small satellites. He co-authored/co-edited 3 books (*Space Antenna Handbook*, Wiley, 2012; *Circularly Polarized Antennas*, IEEE & Wiley, 2014; *Low-Cost Smart Antennas*, Wiley, 2019), over 400 papers and 20 patents. He was a Distinguished Lecturer of IEEE Antennas and Propagation Society, and serves as an Associate Editor for several international Journals (*IEEE Transactions on Antennas and Propagation*; Radio Science; Electronics Letters; IET Circuits, Devices and Systems, etc), and the Editor-in-Chief for John Wiley & Sons Book Series on "Microwave and Wireless Technologies". He served as General Chair of international conferences (LAPC 2013, UCMMT 2021) and was an Invited/Keynote Speaker at many conferences. He is the Lead Guest Editor of *IEEE Trans on Antennas and Propagation* for a Special Issue on "Low-Cost Wide-Angle Beam-Scanning Antennas" (2022), and served as the Lead Guest Editor of Proceedings of the IEEE for a Special Issue on "Small Satellites" (2018), the Lead Guest Editor of *IEEE Trans on Antennas and Propagation* for a Special Issue on "Antennas for Satellite Communication"(2015), and a Guest Editor of IET Circuits, Devices & Systems for a Special Issue in "Photonic and RF Communications Systems" (2014). He is the UK's Representative in European Association on Antennas and Propagation (EurAAP). He is a Fellow of IEEE, a Fellow of Royal Aeronautical Society, and a Fellow of IET.

Benito Sanz-Izquierdo (Member, IEEE) received the B.Sc. degree from ULPGC, Spain, and the M.Sc. and Ph.D. degrees from the University of Kent, U.K.

He was Research Associate with the School of Engineering, University of Kent, in 2013, became a Lecturer in electronic systems, and a Senior Lecturer, in 2018. In 2012, he worked for Harada Industries Ltd., where he developed novel antennas for the automotive industry. His research has been funded through a variety of sources, such as the UK EPSRC, the Royal Academy of Engineering, and the Royal Society. His research interests include multiband antennas, wearable electronics, additive manufacturing (3D printing), substrate integrated waveguides components, metamaterials, electromagnetic band-gap structures, frequency selective surfaces, and reconfigurable devices. He has received awards and recognition for his work on wearable antennas (mention in the House of Lords and the IEEE IWAT Best Paper Award), frequency selective surfaces (best paper at an IET Workshop on Aerospace Applications Award), and reconfigurable antennas (2017 CST University Publication Award for an IEEE TRANSACTIONS Article) amongst others.

Haiwei Zhang received the B.S. and M.S. degrees in electronics engineering from Xidian University in 2009 and 2012, respectively, and the Ph.D. degree in electronics engineering from the City University of Hong Kong in 2016. He joined Huawei Technologies Company, Ltd., in 2016, where he was involved with the development of various antennas and RF components/sub-systems for the 5G and beyond wireless communications. He was awarded the Hong Kong Ph.D. Fellowship in 2012.

Lehu Wen (Member, IEEE) received Ph.D. degree in electronic engineering from the University of Kent, Canterbury, U.K, in 2020.

He is currently a Research Associate with the School of Engineering, University of Kent, Canterbury, U.K. His research interests include wideband dual-polarized antennas, circularly polarized antennas, tightly coupled array antennas, and mobile terminal antennas.

Wei Hu (Member, IEEE) received the Ph.D. degree in electromagnetic fields and microwave technology from Xidian University, Xi'an, China, in 2013.

From 2013 to 2017, he was a lecturer with the National Key Laboratory of Antennas and Microwave Technology, Collaborative Innovation Center of Information Sensing and Understanding, Xidian University, where he is currently an Associate Professor. From 2018 to 2019, he visited the University of Kent, Kent, U.K., as an Academic Visitor. He has authored or coauthored over 80 internationally refereed journal articles and has been serving as a reviewer for a number of technical journals and international conferences.

His current research interests include multiband and wideband antennas, circularly polarized antennas, MIMO antenna arrays, and wideband wide-scanning phased arrays.

Qi Luo (Senior Member, IEEE) is a senior lecturer at the School of Physics, Engineering and Computer Science, University of Hertfordshire, United Kingdom. He received his MSc degree with distinction from the University of Sheffield, the UK in 2006 and his PhD degree from the University of Porto, Portugal with distinction in 2012. From 2012-2013, he worked at the University of Surrey, UK as a research fellow. After that, he worked at the School of Engineering and Digital Arts, University of Kent, the UK as a senior research fellow. His research interests are reflectarrays, transmitarrays, smart antennas, circularly polarized antennas, phased arrays, metasurfaces, multiband microstrip antennas, and electrically small antenna design.

This article has been accepted for publication in IEEE Transactions on Antennas and Propagation. This is the author's version which has not been fully edited and content may change prior to final publication. Citation information: DOI 10.1109/TAP.2022.3209177

> REPLACE THIS LINE WITH YOUR PAPER IDENTIFICATION NUMBER (DOUBLE-CLICK HERE TO EDIT) <   14

Josaphat Tetuko Sri Sumantyo (Senior Member, IEEE) was born in Bandung, Indonesia in 1970. He received the B.Eng. and M.Eng. degrees in electrical and computer engineering (subsurface radar systems) from Kanazawa University, Japan, in 1995 and 1997, respectively, and a Ph.D. degree in artificial system sciences (applied radio wave and radar systems) from Chiba University, Japan, in 2002.

From 2002 to 2005, he was a Lecturer (Postdoctoral Fellowship Researcher) with the Center for Frontier Electronics and Photonics, Venture Business Laboratory, Chiba University, Japan. From 2005 to 2013, he was an Associate Professor (permanent staff) with the Center for Environmental Remote Sensing, Chiba University, where he is currently a Full Professor (permanent staff). He is Head Department of Environmental Remote Sensing and Head Division of Earth and Environmental Sciences, Graduate School of Integrated Science and Technology, Chiba University in 2019-2020 and 2022-2023. Head of Disaster Information Analysis Research Division, Disaster Medical Research Center, Chiba University since 2021. He is also a lecturer in the Department of Electrical Engineering, Faculty of Engineering, Universitas Sebelas Maret (UNS), Indonesia since 2020. His research interest is theoretically scattering microwave analysis and its applications in microwave (radar) remote sensing, especially synthetic aperture radar, quantum radar, noise radar, and subsurface radar (VLF), including InSAR, DInSAR, and PS-InSAR, analysis and design of antennas for mobile satellite communications and microwave sensors, development of microwave sensors, including synthetic aperture radar for UAV, aircraft, high altitude platform system (HAPS), and microsatellite. He published about 930 journal and conference papers, and 15 book-related wave analyses, UAV, SAR, space antenna, and a small antenna. He is General Chair of the 7th and 8th Asia-Pacific Conference on Synthetic Aperture Radar (APSAR 2021 and 2023), and more than 290 Invited Talks and Lectures. He is Co-leader of the Technical Committee of Working Group on Remote Sensing Instrumentation and Technologies for UAV of IEEE-GRSS, Technical Committee on Instrumentation, and Future Technologies (IFT-TC), and Associate Editor of IEEE Geoscience and Remote Sensing Letter (GRSL) since 2021.

Xue-Xia Yang (Senior Member, IEEE) received the B.S. and M.S. degrees from Lanzhou University, Lanzhou, China, in 1991 and 1994, respectively, and the Ph.D. degree in electromagnetic field and microwave technology from Shanghai University, Shanghai, China, in 2001. From 1994 to 1998, she was a Teaching Assistant and a Lecturer with Lanzhou University. From 2001 to 2008, she was a Lecturer and an Associate Professor with Shanghai University. She is currently a Professor and the Head of the Antennas and Microwave Research and Development Center, Shanghai University. She has authored or coauthored over 180 technical journal and conference papers. Her research interests include antennas theory and technology, computational electromagnetics, and microwave power transmission. Dr. Yang is a member of the Committee of Antenna Society of China Electronics Institute and a Senior Member of China Electronics Institute. She is an Associate Editor of the Journal of Shanghai University (Science edition). She is also a frequent reviewer for over ten scientific journals.